#### PAPER IN FOREFRONT



# Laser-induced graphene electrodes for electrochemical ion sensing, pesticide monitoring, and water splitting

Ivan S. Kucherenko<sup>1,2</sup> • Bolin Chen<sup>1</sup> • Zachary Johnson<sup>1</sup> • Alexander Wilkins<sup>3</sup> • Delaney Sanborn<sup>1</sup> • Natalie Figueroa-Felix<sup>1</sup> • Deyny Mendivelso-Perez<sup>3</sup> • Emily A. Smith<sup>3</sup> • Carmen Gomes<sup>1</sup> • Jonathan C. Claussen<sup>1</sup>

Received: 20 February 2021 / Revised: 18 May 2021 / Accepted: 30 June 2021 / Published online: 1 September 2021 © Springer-Verlag GmbH Germany, part of Springer Nature 2021

#### **Abstract**

Laser-induced graphene (LIG) has shown to be a scalable manufacturing route to create graphene electrodes that overcome the expense associated with conventional graphene electrode fabrication. Herein, we expand upon initial LIG reports by functionalizing the LIG with metallic nanoparticles for ion sensing, pesticide monitoring, and water splitting. The LIG electrodes were converted into ion-selective sensors by functionalization with poly(vinyl chloride)-based membranes containing K<sup>+</sup> and H<sup>+</sup> ionophores. These ion-selective sensors exhibited a rapid response time (10–15 s), near-Nernstian sensitivity (53.0 mV/dec for the K<sup>+</sup> sensor and – 56.6 mV/pH for the pH sensor), and long storage stability for 40 days, and were capable of ion monitoring in artificial urine. The pesticide biosensors were created by functionalizing the LIG electrodes with the enzyme horseradish peroxidase and displayed a high sensitivity to atrazine (28.9 nA/μM) with negligible inference from other common herbicides (glyphosate, dicamba, and 2,4-dichlorophenoxyacetic acid). Finally, the LIG electrodes also exhibited a small overpotential for hydrogen evolution reaction and oxygen evolution reaction. The oxygen evolution reaction tests yielded overpotentials of 448 mV and 995 mV for 10 mA/cm<sup>2</sup> and 100 mA/cm<sup>2</sup>, respectively. The hydrogen evolution reaction tests yielded 35 mV and 281 mV for the corresponding current densities. Such a versatile LIG platform paves the way for simple, efficient electrochemical sensing and energy harvesting applications.

**Keywords** Graphene · Biosensor · Pesticide · Ion-selective membrane · Water splitting · Urinalysis

# Introduction

Graphene is a one-atom-thick sheet of carbon atoms arranged in a honeycomb-like structure. It is characterized by a large surface area, high electrical conductivity, high mechanical stiffness, and thermal conductivity [1]. Such properties make

ABC Highlights: authored by Rising Stars and Top Experts.

Ivan S. Kucherenko and Bolin Chen contributed equally to this work.

- ☑ Jonathan C. Claussen jcclauss@iastate.edu
- Mechanical Engineering Department, Iowa State University, Ames, IA 50011, USA
- Institute of Molecular Biology and Genetics of the National Academy of Sciences of Ukraine, 150 Zabolotnogo str., Kyiv 03143, Ukraine
- <sup>3</sup> Chemistry Department, Iowa State University, Ames, IA 50011, USA

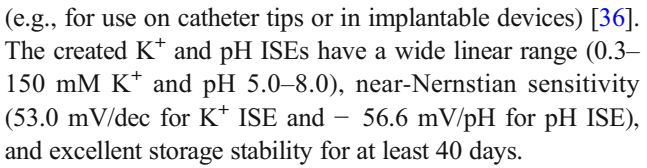
graphene-based electrodes particularly attractive for various electrochemical applications, including ion sensing, amperometric sensing, and water splitting [2, 3]. Traditional methods for the creation of graphene-based materials generally include chemical vapor deposition (CVD) which is a laborious process that requires vacuum chambers and high temperatures (500–1000 °C) [4]. Furthermore, after such CVD synthesis, additional complex procedures are often required to transfer the synthesized graphene to insulating dielectric materials that are suitable for electronic devices [5, 6]. To simplify graphene-based circuit fabrication, researchers have developed a variety of printing techniques including inkjet [7, 8], screen [9], and dispenser printing [10]. Though these techniques generally print exfoliated flakes of graphite (graphene or graphene oxide) that are less conductive than pristine CVDgrown graphene, researchers have developed a variety of postprint annealing techniques (i.e., rapid pulse laser annealing, high-temperature thermal annealing, and photonic annealing) that improve the electrical conductivity to levels near printed metals (< 1 k  $\Omega$ ) [7, 11–13]. Recently, researchers have been



able to effectively combine direct write printing and post-print annealing to create highly conductive graphene circuits via a fabrication method coined laser-induced graphene (LIG) or laser-scribed graphene (LSG) [14–17]. LIG can be produced from carbon-based polymers (i.e., polyimide) by direct write CO<sub>2</sub> laser irradiation which converts the hybridization of carbon within the polymer from sp<sup>3</sup> to sp<sup>2</sup> found in graphene [15]. LIG circumvents the need for ink formulation and post-print annealing involved in graphene printing techniques, uses inexpensive raw materials, and can create electrode designs on-the-fly as circuits can be rapidly created with CAD software and uploaded into the CO<sub>2</sub> laser.

Researchers have been able to functionalize the surface of LIG with nanoparticles and/or biorecognition agents to create a wide variety of electrodes which include those capable of splitting water and water oxidation [18, 19], sensing fertilizer and hydration ions in soil and sweat respectively [20, 21], monitoring of biogenic amines and *Salmonella* bacteria in food samples [16, 22], impedance-based cell monitoring [23], aptamer-based biosensing in serum [17], and biomarkers in sweat [24]. In this manuscript, we will expand upon these reports by demonstrating a simpler approach through the creation of LIG electrodes for water splitting, expanding the research of LIG-based ion sensing to include pH monitoring, and introducing the first example of a pesticide-monitoring LIG-based electrode through functionalization with an enzyme.

Potentiometric ion-selective electrodes (ISEs) have been used for the selective and sensitive (nanomolar detection limits) detection of ions in a wide variety of applications including detecting perchlorate and iodide in water [25, 26], ammonium and potassium in urine [27], and lithium in whole blood [28, 29]. Conventional liquid-junction ISEs contain an aqueous internal reference electrolyte between the working electrode and ion-selective membrane that requires maintenance and creates long-term stability due to leaching. However, solid-contact or solid-state ISEs do not contain such a liquid reference electrolyte which can improve their stability and decrease their maintenance [30]. For the development of solid-contact ISEs, it is important to maintain the stability of the potential at the interface between the ion-selective membrane and the electrode. To reach this goal, sufficiently fast and reversible ion-to-electron transduction should take place at the solid-contact interface [31]. Furthermore, the potential should not be significantly influenced by external interfering factors, such as light, O2, and CO2, and also, the contact area between the membrane and electrode surface should be maximized [32]. LIG-based electrodes satisfy these requirements and are a promising platform for the development of ISEs [20, 33]. In the present work, we develop solid-state ISEs for the detection of K<sup>+</sup> and pH. These targets were selected since their detection plays an important role in environmental sensing [34], human health monitoring [35], and medical diagnostics



In addition to ion sensing, we demonstrate how LIG-based electrodes can be used for pesticide monitoring through functionalization with the enzyme horseradish peroxidase (HRP). Horseradish peroxidase (HRP), a heme group enzyme, has shown selective measurement of hydrogen peroxide through amperometry [23, 37]. Electrodes functionalized with HRP have been used to monitor a wide variety of analytes including glyphosate, atrazine, and dichlofenthion [38–40]. However, we demonstrate that LIG electrodes functionalized with HRP can selectively monitor the herbicide atrazine with high sensitivity (28.9 nA/ $\mu$ M) and report minimal interference from other herbicides commonly applied in the Corn Belt region of the USA including glyphosate, dicamba, and 2,4-dichlorophenoxyacetic acid.

Finally, we demonstrate how LIG-based electrodes can be used in electrochemical energy conversion. Electrochemical electrolysis has gained recent attraction due to its ability to increase hydrogen evolution reaction (HER) and oxygen evolution reaction (OER) kinetics [41–43]. To date, various noble metals and semiconductors prove to be promising HER catalysts. Phosphides [44, 45], sulfides, and manganese have shown good performance in HER. Hydroxides/oxides of nickel [46], iron [46, 47], and cobalt [48] have shown good performance in OER. However, metallic platinum (Pt) remains as one of the most promising used catalysts for electrolysis due to its high catalytic activity in liberating H<sub>2</sub> at high reaction rates and low overpotentials  $(\eta)$ . To reduce the cost but maintain the superior catalytic activity, nanoscale amounts of platinum in the form of platinum nanoparticles (PtNPs) are often deposited onto the electrodes via drop-casting [49], thermal decomposition of Pt salt [18, 50], or atomic layer deposition [51]. However, researchers have recently demonstrated that electroless deposition of PtNPs is a simple one-pot synthesis process offering several advantages compared to commonly used methods to synthesize electrocatalysts. Such methods include solid-phase reaction and hydrothermal, which require delicate control of reaction time and temperature. The developed LIG-Pt and LIG-NiO electrodes display an overpotential at 100 mA/cm<sup>2</sup> of 281 and 995 mV with relatively low Tafel slopes of 82 and 48 mV/dec for HER and OER, respectively.

# **Materials and methods**

# Fabrication of laser-induced graphene electrodes

The LIG electrodes were prepared by irradiation of polyimide (0.125 mm thick, DuPont, USA) by the CO<sub>2</sub> laser (75-watt



Epilog Fusion M2, USA). The polyimide was fixed on a glass substrate and cleaned with a wipe before lasing. Drawings of the electrodes were prepared in CorelDraw and then submitted to the laser-controlling program. Lasing parameters were the following: 7% speed, 7% power, 50% frequency, raster mode, and 600 dpi, and all other parameters were selected as "off." The laser beam was defocused by the placement of the polyimide sheet 2 mm lower than the focus distance. These conditions were experimentally selected to achieve the highest quality of graphene.

# Preparation of ion-selective electrodes

Mixture for the preparation of K<sup>+</sup> ISE contained valinomycin (potassium-selective ionophore, 2.5 mg), dioctyl sebacate (plasticizer, 165 mg), poly(vinyl chloride) high molecular weight (the main solid component of the membrane, 82.5 mg), and tetrahydrofuran (solvent, 1667 mg) [52]. The mixture for the preparation of pH ISE contained hydrogen ionophore I (5 mg), potassium tetrakis(4-chlorophenyl)borate (ionic additive for better ion exchange, 2.5 mg), dioctyl sebacate (327.5 mg), poly(vinyl chloride) high molecular weight (165 mg), and tetrahydrofuran (3163 mg) [53]. After preparation, the mixtures were vortexed for 3 min, left in the fridge (+ 4 °C) overnight for a complete dissolution of the components, and vortexed again for 3 min before usage. The mixtures could be used for several months if stored in the fridge. However, to achieve the best sensor performance, it is better to prepare new mixtures every 2-3 weeks. K<sup>+</sup> and pH ISEs were prepared by drop-casting 8 µL of the corresponding ionophore mixture onto the terminal circular part of the electrode. About 1 mm of the surrounding area (polyimide) was also covered with the mixture to prevent direct contact between the tested solution and the graphene. For the same reason, the central part of the electrode was covered in advance with acrylic polish. The prepared ISEs were stored dry at room temperature.

# Preparation of Horseradish Peroxidase-LIG electrodes

Once LIG electrodes were lased, acrylic polish was applied to the stem of the electrode to act as a passivation layer. Silver paste was applied to the contact of the electrode. A solution of 3% Horseradish Peroxidase (HRP) Type VI (Sigma Aldrich) and 2% glutaraldehyde (weight) was prepared fresh in a 1:1 volumetric ratio. After mixing this solution,  $1~\mu L$  of the mixture was drop-coated onto the pad of the working electrode. The deposited enzyme mixture on the electrode was allowed to dry for 12~h at  $4~^{\circ} C$  before testing.

# Preparation of artificial urine

Artificial urine for testing K<sup>+</sup> and pH ISEs was prepared according to [54] with few modifications. The artificial urine was obtained by dissolving the following components in DI: sodium L-lactate (1.1 mM), sodium citrate dehydrate (2 mM), sodium bicarbonate (25 mM), urea (170 mM), uric acid (0.4 mM), calcium chloride (2.5 mM), sodium chloride (90 mM), magnesium sulfate (2 mM), sodium sulfate (10 mM), sodium dihydrogen phosphate (7 mM), and disodium hydrogen phosphate (7 mM). The solution was filtered through a 0.45-µM syringe filter to remove larger undissolved components. Thus, all ions found endogenously in urine were present in the artificial urine except potassium and ammonium. The pH of the as-prepared artificial urine was 8.5 and was decreased to lower values (pH 5.0, 6.0, 6.5, 7.0, 7.5, 8.0) using hydrochloric acid (HCl).

# **Electrochemical characterization**

Water-splitting electrodes A three-electrode setup was used on a CH Instrument, Inc. (CHI) 6273E electrochemical analyzer (potentiostat), with a CHI115 Pt wire as the counter electrode, CHI111 Ag/AgCl as the reference electrode, and LIG as the working electrode. The tests were performed in 1 M KOH. Linear-sweep voltammetry (LSV) was performed for both the LIG-NiO and LIG-Pt electrodes. The LIG-Ni electrode was tested for the oxygen evolution reaction (OER) from 0 to 1.7 V (vs Ag/AgCl) at a scan rate of 5 mV/s. The LIG-Pt electrode was tested for the hydrogen evolution reaction (HER) from 0 to − 1.7 V (vs Ag/AgCl) at a scan rate of 5 mV/s.

**Ion-selective electrodes** The developed LIG ISEs were electrochemically characterized with a CHI 6273E electrochemical analyzer (potentiostat). The potentiostat operated in "open circuit potentiometry" mode, with 0.5 s interval between separate readings. An ISE was connected to the working connector, and a reference electrode (CHI111 Ag/AgCl liquidjunction reference electrode filled with 1 M KCl) was connected to the combined reference and counter connectors. The ISE and the reference electrode were placed in a 10-mL glass beaker filled with 4 mL of DI with constant stirring (~ 100 RPM) by a magnetic stirrer. For the sensor calibration, aliquots of concentrated KCl solution (1, 10, 100, and 2000 mM in DI) were added to the working cell. The calibration of pH ISEs was carried out in standard pH solutions with pH 4.0, 7.0, and 10 (Fisher Scientific) and in 1 mM phosphate buffer saline (PBS) with different pH levels adjusted with HCl and NaOH.



Horseradish peroxidase-LIG electrodes A three-electrode setup was used on a CHI 6273E electrochemical analyzer with a CH115 platinum wire counter electrode, CH111 Ag/AgCl reference electrode, and functionalized LIG working electrode. Amperometric i-t tests were performed at - 0.1 V. The test cell contained PBS pH 7.4. A calibration experiment for atrazine was conducted by starting the i-t test. Upon reaching steady state, 0.4 mM hydrogen peroxide (H<sub>2</sub>O<sub>2</sub>) was added to the test cell. As the oxidation-reduction reaction occurred between HRP and H<sub>2</sub>O<sub>2</sub>, a signal was detected. Once this signal reached steady state, atrazine was added in 10-µM increments, allowing a steady-state signal to be reached before the next addition. An i-t test was performed for a single sensor by testing the response to each pesticide at 10-µM additions. The test setup was rinsed 2 times with PBS at the end of every test. The same sensor and procedure were used to test for the detection of dicamba, 2,4dichlorophenoxyacetic acid, and glyphosate.

Microscopy characterization Microscopic images were taken from a FEI Quanta 250 FEG Scanning Electron Microscope (SEM) at an operating voltage of 10 kV with EDS. An Oxfords Instruments Aztec X-Max 80 detector system connected to FEI Quanta 250 was used to collect the EDS photons for elemental detection. Raman spectrum was obtained by using an XploRa Plus confocal Raman upright microscope equipped with a 532-nm excitation source and a Synapse Electron Multiplying Charge Coupled Device camera (Horiba Scientific/NJ, France). The intensity (height) was

determined for the D, G, and 2D bands by fitting the data to a Lorentzian model. XPS measurements were performed using a PHI ESCA 5500 instrument. The sample was irradiated with 200 W unmonochromated Al K $\alpha$  X-rays. CasaXPS was used to process raw data files.

#### Results and discussion

# **Characterization of the LIG electrodes**

The LIG electrodes used for these tests were produced by etching 0.125 mm polyimide (PI) with a CO<sub>2</sub> laser as shown in Fig. 1. After lasing, a dielectric coating was applied on the sample with only the disk-shape working area (dia. 5 mm) exposed. The ISEs were prepared by drop-coating ion-selective membranes selective to K<sup>+</sup> and pH on the working area followed by conditioning overnight to stabilize the sensors and improve the detection limit [28]. The HRP sensors were prepared by drop-coating enzyme mixture on the working electrode followed by drying for 12 h. Refer to the "Materials and methods" section for a summary of the fabrication process. The fabrication of water-splitting electrodes included thermal decomposition of nickel (II) acetate tetrahydrate and an electroless deposition method for the platinum (Pt). Refer to the Supplementary information section for water-splitting electrode fabrication.

Scanning electron microscopy (SEM) images with corresponding EDS were acquired to investigate the morphology of the LIG electrodes. The pristine LIG shows a porous structure

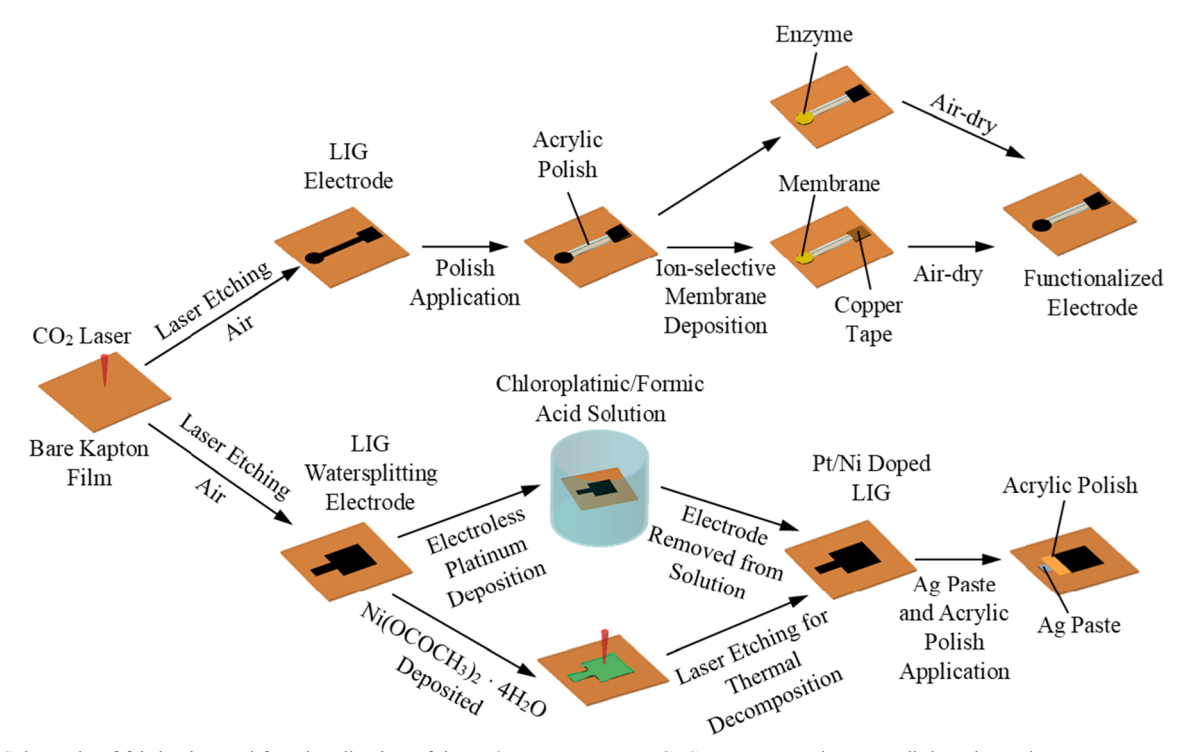


Fig. 1 Schematic of fabrication and functionalization of the LIG HRP sensors, LIG ISE sensors, and water-splitting electrodes



with pores ranging from 200 nm to 10 um (see Supplementary information (ESM) Fig. S1a). ESM Fig. S1b shows the structure of the nickel (II) deposition on the graphene. Similarly, ESM Fig. S1c shows the structure of the platinum (II) deposition. Thermal decomposition of nickel acetate tetrahydrate into nickel oxide (NiO) requires a temperature of at least 380 °C. The LIG-NiO also shows an increase of porosity (ESM Fig. S1b), which could be attributed to the thermal reduction of graphene during the deposition of NiO. This was not observed on the Pt-LIG sample as shown in ESM Fig. S1c. The corresponding EDS was performed to confirm elements present in the NiO-LIG sample as shown in ESM Fig. S2b containing carbon, oxygen, and nickel. The carbon can be found across the sample confirming the successful conversion of PI into LIG by laser irradiation. The nickel and oxygen can be found in the same area which confirm the presence of NiO on the LIG surface.

Pt was electrolessly deposited onto the LIG by immersing the sample into a chloroplatinic acid solution following the protocol that was previously developed in our group [55–57]. The method can deposit platinum onto various surfaces, such as carbon-based materials (carbon nanotube, carbonized wood, graphene) and others like cellulose and SiO<sub>2</sub> wools with surface functionalization [55, 56, 58]. After 20 h, a layer of Pt deposits onto the surface of LIG as shown in ESM Fig. S1c. The EDS was conducted on Pt-LIG samples to confirm the presence of Pt deposition as shown in ESM Fig. S3b. The Raman characterization was performed to confirm the presence of graphene in LIG (ESM Fig. S1d). Three prominent peaks were observed on the LIG: the D peak at ~ 1350 cm<sup>-1</sup> induced by defects or bent sp<sup>2</sup>- carbon bonds, the first-order allowed G peak at  $\sim 1580 \text{ cm}^{-1}$ , and the 2D peak at ~ 2700 cm<sup>-1</sup> originating from second-order zone-boundary phonons [59]. The intensity (height) was determined for the D, G, and 2D bands by fitting the data to a Lorentzian model. The presence of this 2D band in the Raman spectra suggests graphitization of the polyimide substrate and formation of graphene layers due to the high local heating by the CO<sub>2</sub> laser. It shows the  $I_D/I_G$  ratio of 1.2  $\pm$  0.2 and  $I_{2D}/I_G$  ratio of 0.28  $\pm$ 0.04. XPS was also performed on water-splitting catalyst to confirm the elemental composition and chemical valance states. For the LIG-NiO, metallic Ni and Ni<sup>2+</sup> are present with the main peaks located at  $\sim 852.8$  eV,  $\sim 855.03$  eV, and  $\sim$ 860.53 eV. The metallic Ni and the Ni<sup>2+</sup> are about 21% and 79%, respectively (ESM Fig. S1f). The presence of metallic Ni could be attributed to the reduction of Ni<sup>2+</sup> at elevated temperatures [19]. For the LIG-Pt, Pt in the + 2 and + 4 states is present with the main peaks located at  $\sim 73.65$  eV and  $\sim$ 77 eV for Pt(II) and  $\sim$  75.82 eV and  $\sim$  79.17 eV for Pt(IV) (ESM Fig. S1e). The + 2 and the + 4 state has about 18% and 82%, respectively, which we postulate to be PtO and PtO<sub>2</sub>.

Electrochemical performance of LIG was characterized by cyclic voltammetry in 5 mM ferricyanide-ferrocyanide mixture. Eleven electrodes from the same batch were tested (Fig. 2) and showed similar shape of voltammograms and peak currents with little batch-to-batch variation. Peak-topeak separation was about 90 mV, which is similar or better than achieved with other carbon nanomaterials and indicates excellent electrochemical performance of the electrode. For example, the following peak-to-peak separations were reported for electrodes based on various carbon nanomaterials: 68 mV (pyrolytic graphite) [60], 81 mV (LIG) [61], 90 mV (single-walled carbon nanotubes modified with Pt nanospheres) [62], 92 mV (single-walled carbon nanotubes modified with Pd nanocubes) [62], 96 mV (single-walled carbon nanotubes) [63], 183 mV (pyrolytic graphite) [60], 230 mV (multi-walled carbon nanotubes) [63], and 630 mV (pyrolytic graphite) [64].

Other advantages of the developed LIG electrodes include the fast and easy production process (12–15 s to lase one electrode) and low cost of materials. For comparison, commercial CVD-grown graphene film (1  $\times$  1 cm², 4 items) costs \$352 (Sigma-Aldrich, ref. #773719). Recently reported electrodes based on carbon nanotubes and characterized by the authors as simple and fast in production required a 5-step preparation process that lasts  $\sim$  6–8 h [65]. Graphene modified with MoS2 nanocrystals was synthesized during a 45-s microwave annealing of the reaction mixture (MoCl5, graphene oxide, thiourea, and ethanol) using a conventional microwave oven [66].

# Potassium (K<sup>+</sup>) and pH ion-selective sensors

Calibration of K<sup>+</sup> ISEs was carried out in DI by sequentially increasing the KCl concentration in the working cell (Fig. 2c, black line). As a control, a bare LIG electrode was also calibrated (Fig. 2c, red line). As seen, K<sup>+</sup> ISEs respond rapidly after the addition of KCl with a response time of 10–15 s. The response moves in the positive direction since K<sup>+</sup> cations bind with the ionophore and increase the potential of the ion-selective membrane. On the contrary, the bare electrode does not show a stable response to KCl and demonstrates a decrease of potential probably due to higher binding of Cl<sup>-</sup> anions to the graphene surface.

A typical calibration curve of the  $K^+$  ISE is shown on Fig. 2d. The linear range of  $K^+$  detection is from 0.3 mM to at least 150 mM, and the average sensitivity is 53.0 mV/dec. The limit of  $K^+$  detection is 0.1 mM.  $K^+$  concentrations above 150 mM were not tested since they usually cannot be found in real samples. The presented characteristics allow the detection of any  $K^+$  concentration found in urine.

Storage stability of the sensors was also investigated. For this experiment, K<sup>+</sup> ISEs were calibrated after preparation and



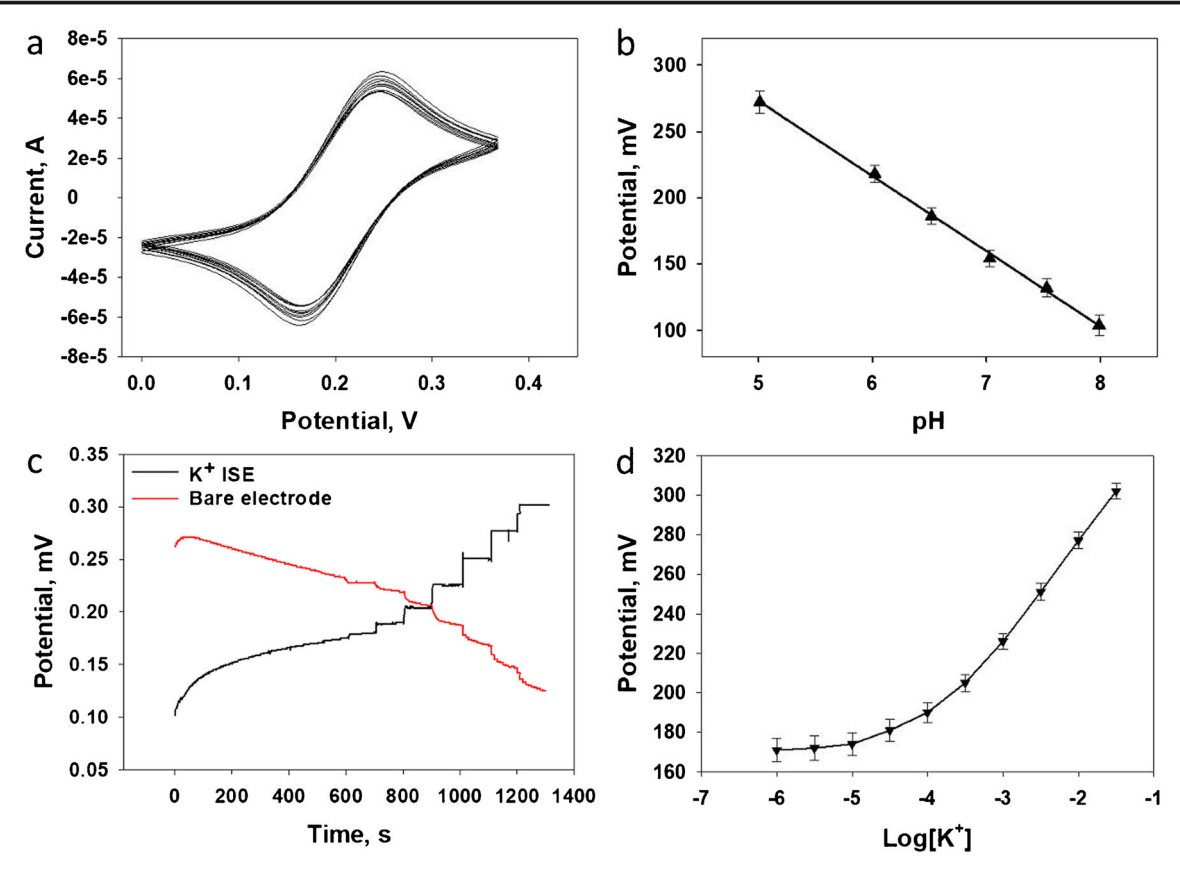


**Fig. 2 a** Cyclic voltammograms of 11 bare LIG electrodes in ferricyanide-ferrocyanide mixture. Voltammetry settings: initial potential + 0.4 V, low potential 0 V, scan rate 10 mV/s, sample interval 0.001 V, and sensitivity 1e-4 A/V. **b** Typical calibration curve of the pH ISE. **c** 

Real signal of the K<sup>+</sup> ISE (black line) and bare LIG electrode (red line) to the sequential additions of KCl (from  $10^{-6}$  to  $10^{-1}$  M, with  $10^{-0.5}$  step). **d** Typical calibration curve of the K<sup>+</sup> ISE

after 40 days of dry storage at room temperature (20–22 °C). Sensitivity of the sensors remained the same, which indicates excellent storage stability.

The characteristics of the developed K<sup>+</sup> ISE are similar to those of other solid-state electrodes found in literature. For example, solid-state K<sup>+</sup> ISEs based on a graphene-covered paper electrode had a sensitivity of 57 mV/dec [21]. Another sensor based on a graphene-coated glassy carbon electrode had a sensitivity of 59.2 mV/dec and was stable during 3 weeks [67]. Sensitivity of K<sup>+</sup> ISEs based on a fullerene-modified glassy carbon electrode was 55 mV/dec [68].

A calibration of pH ISE was carried out in a wide-range buffer (5 mM tris, 5 mM NaH<sub>2</sub>PO<sub>4</sub>, 5 mM sodium citrate, 5 mM boric acid, and pH adjusted with HCl/NaOH) (Fig. 2b). A decrease of pH level leads to the decrease of the ISE potential due to the lower amount of H<sup>+</sup> in the ion-selective membrane. The response was linear within pH 5.0–8.0 which is notably the normal pH range in humans, and the calibration curve was described by the equation y = -56.63x + 556 [69, 70]. Thus, the sensitivity of the sensor was -56.6 mV/pH. Storage stability of the sensors was investigated in the same way as for K<sup>+</sup> ISEs. After 44 days of dry storage, sensitivity of the sensors decreased by 1.5 mV/pH. Thus, the pH ISEs were

a little less stable than the  $K^+$  ISEs but still could be efficiently used after storage.

The obtained results appear to approve upon existing solidstate pH sensors. For example, pH ISEs based on Pt electrodes with a PEDOT polymer had an initial sensitivity of – 46 mV/ pH, which decreased by 55% after 28 days of storage [71]. Another pH ISE based on Pt electrodes with poly(aniline) had sensitivities of 55–59 mV/pH (depending on the ionophore) and remained stable for 1 month [72]. A pH ISE based on a graphite rod demonstrated a sensitivity of – 55 mV/pH and was stable during 2 months [73]. Graphene-based pH ISEs had a sensitivity of – 56 mV/pH, but its storage stability was not tested [21].

# Measurements of K<sup>+</sup> concentration and pH in artificial urine

To evaluate the performance of the sensors in conditions close to real applications, we analyzed artificial urine, prepared as described in the "Materials and methods." Five samples of artificial urine with different pH and K<sup>+</sup> contents were used; the pH and K<sup>+</sup> concentrations were chosen from their typical values in urine (reference range for K<sup>+</sup> concentration in urine



**Table 1** Results of the detection of K<sup>+</sup> concentration and pH level in artificial urine using LIG ISEs

#	Added K <sup>+</sup> concentration, mM	Detected K <sup>+</sup> concentration, mM	Recovery,	pH, measured by pH meter	pH, measured by pH ISE	Recovery,
1	10.0	11.3	113	6.71	7.08	106
2	25.0	22.6	90	7.10	7.44	105
3	50.0	47.0	94	6.11	6.53	107
4	125.0	108.9	87	6.51	6.97	107
5	10.0	9.8	98	7.10	7.40	104

is 25–125 mmol/day and typical pH range is 4.5–8.0 [74]). The results are presented in Table 1. The difference between the spiked potassium concentration and detected concentration by K<sup>+</sup> ISE was 13% or less. The pH ISE detected higher levels of pH than a commercial pH meter; the difference was 0.3–0.4 pH values. This shift is probably explained by the influence of high ionic content of artificial urine on the sensor's working portion. However, for medical purposes, the accuracy of pH detection can be considered sufficient, since the urine pH is highly variable and, in case of diseases, it can be shifted to 1 pH value or even more. Furthermore, accuracy of the pH and K<sup>+</sup> detection may possibly perform better in less complex samples or in diluted urine.

# HRP sensors for atrazine sensing

Amperometric sensing of the herbicide atrazine on the LIG platform was demonstrated. Graphene sensors perform well in terms of enzymatic-based sensing due to the direct electron communication between the electrode and the active center of the enzyme [37]. Horseradish peroxidase was selected for this enzymatic biosensor due to its high stability and availability [75]. Our procedures involve the initial detection of hydrogen peroxide. HRP has shown selective measurements of hydrogen peroxide through amperometry [37]. HRP is a heme group enzyme where the Fe(III) of this group acts as the electron source [23]. Peroxidases are shown to decompose hydrogen peroxide (H<sub>2</sub>O<sub>2</sub>) into water and oxygen [76]. HRP has been used similarly in detecting the herbicide glyphosate at low concentrations [40]. Therefore, it is reasonable to use HRP in detecting our analyte in PBS pH 7.4.

The atrazine calibration curve in Fig. 3a shows the response change to 10- $\mu$ M additions of atrazine followed by a PBS addition of the same volume. The detection mechanism utilized hydrogen peroxide as the substrate. Once a signal was generated due to the decomposition of  $H_2O_2$ , an herbicide would be added in 10- $\mu$ M increments. It is evident that HRP shows a higher affinity toward atrazine over the other herbicides tested. Using the 3-sigma limit of detection, the theoretical limit of detection for this sensor is 1.6  $\mu$ M (Fig. 3b). A variety of common herbicides were tested for interference and enzyme selectivity. Of these herbicides, glyphosate, dicamba, and 2,4-dichlorophenoxyacetic acid were tested. After each run, a different herbicide would be tested on the same sensor. The interferant data is shown in Fig. 3c.

# LIG-Pt/LIG-NiO electrode for water splitting

The HER electrode was prepared by electroless deposition of a nanoscale amount of Pt onto the LIG. The OER electrode was prepared by thermally decomposing the nickel (II) acetate tetrahydrate by photonic heating. The electrocatalytic activities of LIG-Pt and LIG-NiO toward HER and OER in 1 M KOH were measured. Linear-sweep voltammograms (LSV) were performed from 0 to - 1.7 V and 0 to 1.7 V at 5 mV/s for HER and OER, respectively. The catalytic activity of the LIG-Pt and LIG-NiO are plotted in Fig. S4a-b. Analysis of this data includes the conversion of the voltage potential in Ag/AgCl to overpotential in volts vs RHE. The LIG-Pt shows nearly zero onset potential vs RHE, which demonstrated the excellent activity. Overpotentials for current densities of 10 mA/cm<sup>2</sup> and 100 mA/cm<sup>2</sup> are commonly used to compare

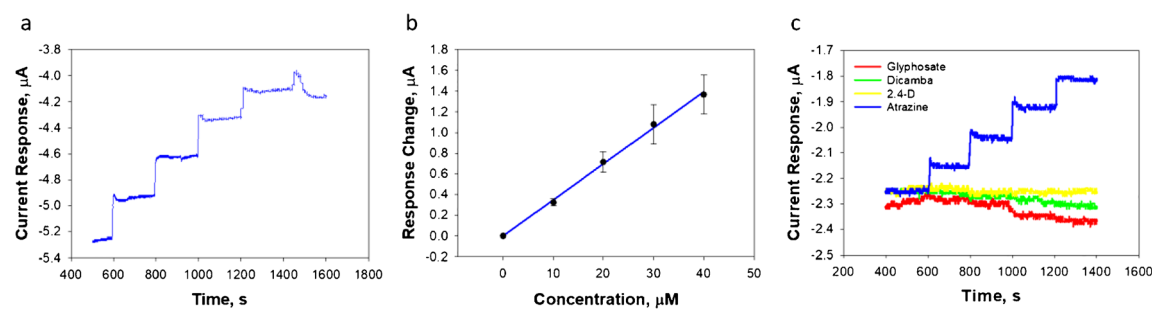


Fig. 3 a Atrazine calibration curve, b electrode sensitivity to atrazine, c interference test of select herbicides

the efficiency of various systems. The OER tests yielded overpotentials of 448 mV and 995 mV for 10 mA/cm<sup>2</sup> and 100 mA/cm<sup>2</sup>, respectively. The HER tests yielded 35 mV and 281 mV for the corresponding current densities. However, the bare LIG (black curve in ESM Fig. S4a-b) does not show a significant current increase in both the HER and OER cases. Another source of comparison is the Tafel slope. The respective OER and HER Tafel slopes were 48 mV/dec and 82 mV/ dec as shown in ESM Fig. S4c-d. The Tafel slope of LIG-Pt is slightly higher than the Pt-based electrode prepared by conventional methods. However, the straightforward electroless deposition method presented here is noteworthy, as it eliminates the need to prepare inks that contain noble metal power, conductive filler, and binder. The Tafel slope of LIG-NiO is as low as 48 mV/dec, indicating the rapid reaction kinetics on the electrode. This value is similar to recently reported values [18]. Hence, LIG with liquid phase deposited metal nanoparticles is an important addition to metal-based electrocatalysts.

# **Conclusions**

In conclusion, we report the fabrication of electrochemical ion sensors, pesticide biosensors, and water-splitting electrodes by utilizing a laser-induced graphene (LIG) platform. The ISE sensors demonstrated wide linear ranges (0.3–150 mM K<sup>+</sup> and pH 5.0–8.0), near-Nernstian sensitivity (53.0 mV/ dec for K+ ISE and - 56.6 mV/pH for pH ISE), and good dry-storage stability (100% of the initial sensitivity after 40 days for K<sup>+</sup> ISE and 97% after 44 days for pH ISE). These analytical characteristics of the sensors are comparable or exceed previous reports for nanomaterial-based K<sup>+</sup> [67] and pH [71, 73] solid-state sensors. Practical applicability of the proposed ISEs was confirmed by the analysis of artificial urine that contained 11 metabolites and inorganic ions. The characteristics of the sensors make them potentially suitable for various biological applications, such as detection of K<sup>+</sup> and pH levels in blood plasma [71, 77], urine [78], and other biological fluids [79, 80]. Simple and efficient LIG electrodes were developed for potentiometric sensing and water splitting. The HRP pesticide biosensors created by functionalizing the LIG electrodes permitted the selective monitoring of the herbicide atrazine with a high sensitivity (28.9 nA/µM) with negligible inference from other common herbicides (glyphosate, dicamba, and 2,4-dichlorophenoxyacetic acid). The LIG electrodes also exhibited small overpotentials of 35 mV for HER and 448 mV for OER at 10 mA/cm<sup>2</sup> after platinum and nickel oxide are immobilized. LIG can be used as electrodes directly after lasing, without necessity in any further treatments that are required in the case of printed graphene electrodes [52]. The fabrication procedure is easily scalable for mass production of the electrodes. Such a low-cost, fast, and simple one-step procedure for the electrode preparation also eliminates the need in modification of the electrode with nanomaterials as was necessary in earlier works [21, 67, 71]. In summary, the presented LIG electrodes can serve as a versatile platform for the creation of solid-state ISEs, enzymatic electrochemical sensing, and water-splitting applications. Additionally, laser induction of polyamide as a fast process could fabricate electrodes on a large scale. The solution phase deposition of a metal precursor could also be integrated into roll-to-roll production of such electrodes, which is amenable to potential scale-up and commercialization.

**Supplementary Information** The online version contains supplementary material available at https://doi.org/10.1007/s00216-021-03519-w.

Acknowledgements J.C.C. and C.L.G. gratefully acknowledges funding support for this work by the National Science Foundation under award number ECCS-1841649 and CMMI-2037026 as well as from the National Institute of Food and Agriculture, U.S. Department of Agriculture, under award number 2020-67021-31375, 2021-67021-34457, and 2021-67011-35130, and by the by the Office of Naval Research under award number N000142012375.

Author contribution Ivan S. Kucherenko: validation, investigation, writing—original draft. Bolin Chen: validation, investigation, writing—original draft. Zachary Johnson: investigation, writing—review and editing. Alexander Wilkins: investigation. Delaney Sanborn: investigation. Natalie Figueroa-Felix: investigation. Deyny Mendivelso-Perez: investigation. Emily A. Smith: investigation. Carmen Gomes: supervision, project administration, conceptualization. Jonathan C. Claussen: supervision, project administration, conceptualization, writing—review and editing.

# **Declarations**

**Competing interests** The authors declare no competing interests.

# References

- Tang L, Wang Y, Li Y, Feng H, Lu J, Li J. Preparation, structure, and electrochemical properties of reduced graphene sheet films. Adv Funct Mater. 2009;19(17):2782–9.
- Yan R, Qiu S, Tong L, Qian Y. Review of progresses on clinical applications of ion selective electrodes for electrolytic ion tests: from conventional ISEs to graphene-based ISEs. Chem Speciat Bioavailab. 2016;28(1-4):72-7.
- Albero J, Mateo D, García H. Graphene-based materials as efficient photocatalysts for water splitting. Molecules. 2019;24(5):906.
- Zhang Y, Zhang L, Zhou C. Review of chemical vapor deposition of graphene and related applications. Acc Chem Res. 2013;46(10): 2329–39.
- Unarunotai S, Murata Y, Chialvo CE, Kim H, MacLaren S, Mason N, et al. Transfer of graphene layers grown on SiC wafers to other substrates and their integration into field effect transistors. Appl Phys Lett. 2009;95(20):202101.
- Bae S, Kim H, Lee Y, Xu X, Park J-S, Zheng Y, et al. Roll-to-roll production of 30-inch graphene films for transparent electrodes. Nat Nanotechnol. 2010;5(8):574

  –8.



- Das SR, Nian Q, Cargill AA, Hondred JA, Ding S, Saei M, et al. 3D nanostructured inkjet printed graphene: via UV-pulsed laser irradiation enables paper-based electronics and electrochemical devices. Nanoscale. 2016;8(35):15870–9.
- Moya A, Gabriel G, Villa R, Javier del Campo F. Inkjet-printed electrochemical sensors. Curr Opin Electrochem. 2017;3(1):29–39.
- Huang X, Leng T, Zhu M, Zhang X, Chen J, Chang K, et al. Highly flexible and conductive printed graphene for wireless wearable communications applications. Sci Rep. 2016;5(1):18298.
- Fu K, Wang YY, Yan C, Yao Y, Chen Y, Dai J, et al. Graphene oxide-based electrode inks for 3D-printed lithium-ion batteries. Adv Mater. 2016;28(13):2587–94.
- Das SR, Srinivasan S, Stromberg LR, He Q, Garland N, Straszheim WE, et al. Superhydrophobic inkjet printed flexible graphene circuits via direct-pulsed laser writing. Nanoscale. 2017;9(48):19058– 65
- Secor EB, Prabhumirashi PL, Puntambekar K, Geier ML, Hersam MC. Inkjet printing of high conductivity, flexible graphene patterns. J Phys Chem Lett [Internet]. 2013;4(8):1347–51 Available from: https://pubs.acs.org/sharingguidelines.
- Secor EB, Ahn BY, Gao TZ, Lewis JA, Hersam MC. Rapid and versatile photonic annealing of graphene inks for flexible printed electronics. Adv Mater. 2015;27(42):6683–8.
- Lin J, Peng Z, Liu Y, Ruiz-Zepeda F, Ye R, Samuel ELG, et al. Laser-induced porous graphene films from commercial polymers. Nat Commun. 2014;5:5714.
- Ye R, James DK, Tour JM. Laser-induced graphene. Acc Chem Res. 2018;51(7):1609–20.
- Vanegas D, Patiño L, Mendez C, Oliveira D, Torres A, Gomes C, et al. Laser scribed graphene biosensor for detection of biogenic amines in food samples using locally sourced materials. Biosensors [Internet]. 2018;8(2):42 Available from: http://www.mdpi.com/2079-6374/8/2/42.
- Fenzl C, Nayak P, Hirsch T, Wolfbeis OS, Alshareef HN, Baeumner AJ. Laser-scribed graphene electrodes for aptamerbased biosensing. ACS Sensors [Internet]. 2017;2(5):616–20 Available from: https://pubs.acs.org/sharingguidelines.
- Zhang J, Zhang C, Sha J, Fei H, Li Y, Tour JM. Efficient watersplitting electrodes based on laser-induced graphene. ACS Appl Mater Interfaces. 2017;9(32):26840–7.
- Zhang J, Ren M, Li Y, Tour JM. In situ synthesis of efficient water oxidation catalysts in laser-induced graphene. ACS Energy Lett. 2018;3(3):677–83.
- Garland NT, McLamore ES, Cavallaro ND, Mendivelso-Perez D, Smith EA, Jing D, et al. Flexible laser-induced graphene for nitrogen sensing in soil. ACS Appl Mater Interfaces [Internet]. 2018;10(45):39124–33 Available from: www.acsami.org.
- An Q, Gan S, Xu J, Bao Y, Wu T, Kong H, et al. A multichannel electrochemical all-solid-state wearable potentiometric sensor for real-time sweat ion monitoring. Electrochem Commun. 2019;107: 106553.
- Soares RRA, Hjort RG, Pola CC, Parate K, Reis EL, Soares NFF, et al. Laser-induced graphene electrochemical immunosensors for rapid and label-free monitoring of Salmonella enterica in chicken broth. ACS Sensors. 2020;5(7):1900–11.
- Tao Z, Raffel RA, Souid A-K, Goodisman J. Kinetic studies on enzyme-catalyzed reactions: oxidation of glucose, Decomposition of Hydrogen Peroxide and Their Combination. Biophys J. 2009;96(7):2977–88.
- Yang Y, Song Y, Bo X, Min J, Pak OS, Zhu L, et al. A laser-engraved wearable sensor for sensitive detection of uric acid and tyrosine in sweat. Nat Biotechnol. 2020;38(2):217–24.
- Kim Y, Amemiya S. Stripping analysis of nanomolar perchlorate in drinking water with a voltammetric ion-selective electrode based on thin-layer liquid membrane. Anal Chem. 2008;80(15):6056–65.

- Malon A, Radu A, Qin W, Qin Y, Ceresa A, Maj-Zurawska M, et al. Improving the detection limit of anion-selective electrodes: An iodide-selective membrane with a Nanomolar detection limit. Anal Chem. 2003;75(15):3865–71.
- Kucherenko IS, Sanborn D, Chen B, Garland N, Serhan M, Forzani E, et al. Ion-selective sensors based on laser-induced graphene for evaluating human hydration levels using urine samples. Adv Mater Technol. 2020;5(6):1901037.
- Hu J, Stein A, Bühlmann P. Rational design of all-solid-state ionselective electrodes and reference electrodes. TrAC, Trends Anal. Chem. 2016;76:102–14.
- Novell M, Guinovart T, Blondeau P, Rius FX, Andrade FJ. A paper-based potentiometric cell for decentralized monitoring of Li levels in whole blood. Lab Chip [Internet]. 2014;14(7):1308–14 [cited 2021 Feb 16] Available from: www.rsc.org/loc.
- Lindner E, Gyurcsányi RE. Quality control criteria for solid-contact, solvent polymeric membrane ion-selective electrodes. J Solid State Electrochem. 2009 Jan;13(1):51–68.
- Nikolskii BP, Materova EA. Solid contact in membrane ionselective electrodes. Ion-selective electrode Rev. 1985;7(1):3–39.
- van de Velde L, d'Angremont E, Olthuis W. Solid contact potassium selective electrodes for biomedical applications – a review. 160, Talanta. 2016;160:56–65.
- Kurra N, Jiang Q, Nayak P, Alshareef HN. Laser-derived graphene: a three-dimensional printed graphene electrode and its emerging applications. Nano Today. 2019;24:81–102.
- Zuliani C, Diamond D. Opportunities and challenges of using ionselective electrodes in environmental monitoring and wearable sensors. Electrochim Acta. 2012;84:29–34.
- Kucherenko IS, Sanborn D, Chen B, Garland N, Serhan M, Forzani E, et al. Ion-selective sensors based on laser-induced graphene for evaluating human hydration levels using urine samples. Adv Mater Technol. 2020;5(6):1901037.
- Dimeski G, Badrick T, John AS. Ion selective electrodes (ISEs) and interferences—a review. Clin Chim Acta. 2010;411(5–6):309–17.
- Shao Y, Wang J, Wu H, Liu J, Aksay IA, Lin Y. Graphene based electrochemical sensors and biosensors: a review. Electroanalysis [Internet]. 2010;22(10):1027–36. [cited 2020 Jan 3] Available from: https://doi.org/10.1002/elan.200900571.
- Bucur B, Munteanu FD, Marty JL, Vasilescu A. Advances in enzyme-based biosensors for pesticide detection, vol. 8. Biosensors: MDPI AG; 2018. p. 27.
- Keay RW, McNeil CJ. Separation-free electrochemical immunosensor for rapid determination of atrazine. Biosens Bioelectron. 1998;13(9):963–70.
- Songa EA, Arotiba OA, Owino JHO, Jahed N, Baker PGL, Iwuoha EI. Electrochemical detection of glyphosate herbicide using horseradish peroxidase immobilized on sulfonated polymer matrix. Bioelectrochemistry. 2009;75(2):117–23.
- Roger I, Shipman MA, Symes MD. Earth-abundant catalysts for electrochemical and photoelectrochemical water splitting. Nat Rev Chem. 2017;1:0003.
- Wang J, Cui W, Liu Q, Xing Z, Asiri AM, Sun X. Recent progress in cobalt-based heterogeneous catalysts for electrochemical water splitting. Adv Mater. 2016;28(2):215–30.
- 43. Anantharaj S, Ede SR, Sakthikumar K, Karthick K, Mishra S, Kundu S. Recent trends and perspectives in electrochemical water splitting with an emphasis on sulfide, selenide, and phosphide catalysts of Fe, Co, and Ni: a review. ACS Catal. 2016;6:8069–97.
- Buss JA, Hirahara M, Ueda Y, Agapie T. Molecular mimics of heterogeneous metal phosphides: thermochemistry, hydrideproton isomerism, and HER reactivity. Angew Chem Int Ed. 2018;57(50):16329–33.
- Tan Y, Wang H, Liu P, Shen Y, Cheng C, Hirata A, et al. Versatile nanoporous bimetallic phosphides towards electrochemical water splitting. Energy Environ Sci. 2016;9(7):2257–61.



 Trotochaud L, Young SL, Ranney JK, Boettcher SW. Nickel-iron oxyhydroxide oxygen-evolution electrocatalysts: the role of intentional and incidental iron incorporation. J Am Chem Soc. 2014;136(18):6744–53.

- Zhang B, Lui YH, Gaur APS, Chen B, Tang X, Qi Z, et al. Hierarchical FeNiP@ultrathin carbon nanoflakes as alkaline oxygen evolution and acidic hydrogen evolution catalyst for efficient water electrolysis and organic decomposition. ACS Appl Mater Interfaces. 2018;10(10):8739–48.
- Zhang B, Qi Z, Wu Z, Lui YH, Kim TH, Tang X, et al. Defect-rich
   D material networks for advanced oxygen evolution catalysts.
   ACS Energy Lett. 2019;4(1):328–36.
- Feng LL, Fan M, Wu Y, Liu Y, Li GD, Chen H, et al. Metallic Co9S8 nanosheets grown on carbon cloth as efficient binder-free electrocatalysts for the hydrogen evolution reaction in neutral media. J Mater Chem A. 2016;4(18):6860–7.
- Song X, Zhao H, Fang K, Lou Y, Liu Z, Liu C, et al. Effect of platinum electrode materials and electrolysis processes on the preparation of acidic electrolyzed oxidizing water and slightly acidic electrolyzed water. RSC Adv. 2019;9(6):3113–9.
- Nayak P, Jiang Q, Kurra N, Wang X, Buttner U, Alshareef HN. Monolithic laser scribed graphene scaffolds with atomic layer deposited platinum for the hydrogen evolution reaction. J Mater Chem A. 2017;5(38):20422–7.
- He Q, Das SR, Garland NT, Jing D, Hondred JA, Cargill AA, et al. Enabling inkjet printed graphene for ion selective electrodes with postprint thermal annealing. ACS Appl Mater Interfaces. 2017;9(14):12719–27.
- Zhang J, Guo Y, Li S, Xu H. A solid-contact pH-selective electrode based on tridodecylamine as hydrogen neutral ionophore. Meas Sci Technol. 2016;27(10):105101.
- Brooks T, Keevil CW. A simple artificial urine for the growth of urinary pathogens. Lett Appl Microbiol. 1997;24(3):203–6.
- Chen B, Garland NT, Geder J, Pruessner M, Mootz E, Cargill A, et al. Platinum nanoparticle decorated SiO 2 microfibers as catalysts for micro unmanned underwater vehicle propulsion. ACS Appl Mater Interfaces. 2016;8(45):30941–7.
- Marr KM, Chen B, Mootz EJ, Geder J, Pruessner M, Melde BJ, et al. High aspect ratio carbon nanotube membranes decorated with Pt nanoparticle urchins for micro underwater vehicle propulsion via H<inf>2</inf>O<inf>2</inf> decomposition. ACS Nano. 2015;9(8):7791–803.
- Claussen JC, Daniele MA, Geder J, Pruessner M, Makinen AJ, Melde BJ, et al. Platinum-paper micromotors: an urchin-like nanohybrid catalyst for green monopropellant bubble-thrusters. ACS Appl Mater Interfaces. 2014;6(20):17837–47.
- Chen B, Gsalla A, Gaur A, Lui YH, Tang X, Geder J, et al. Porous wood monoliths decorated with platinum nano-urchins as catalysts for underwater micro-vehicle propulsion via H 2 O 2 decomposition. ACS Appl Nano Mater. 2019;2(7):4143–9.
- Ferrari AC, Meyer JC, Scardaci V, Casiraghi C, Lazzeri M, Mauri F, et al. Raman spectrum of graphene and graphene layers. Phys Rev Lett. 2006;97(18):187401.
- Brownson DAC, Smith GC, Banks CE. Graphene oxide electrochemistry: the electrochemistry of graphene oxide modified electrodes reveals coverage dependent beneficial electrocatalysis. R Soc Open Sci. 2017;4(11):171128.
- Liu J, Zhang L, Yang C, Tao S. Preparation of multifunctional porous carbon electrodes through direct laser writing on a phenolic resin film. J Mater Chem A. 2019;7(37):21168–75.

- Ye R, Peng Z, Wang T, Xu Y, Zhang J, Li Y, et al. In situ formation of metal oxide nanocrystals embedded in laser-induced graphene. ACS Nano. 2015;9(9):9244–51.
- Li J, Cassell A, Delzeit L, Han J, Meyyappan M. Novel threedimensional electrodes: electrochemical properties of carbon nanotube ensembles. J Phys Chem B. 2002;106(36):9299–305.
- Moore RR, Banks CE, Compton RG. Basal plane pyrolytic graphite modified electrodes: comparison of carbon nanotubes and graphite powder as electrocatalysts. Anal Chem. 2004;76(10):2677–82.
- Kim JH, Hwang J-Y, Hwang HR, Kim HS, Lee JH, Seo J-W, et al. Simple and cost-effective method of highly conductive and elastic carbon nanotube/polydimethylsiloxane composite for wearable electronics. Sci Rep. 2018;8(1):1375.
- Youn DH, Jang JSJ-W, Kim JY, Jang JSJ-W, Choi SH, Lee JS. Fabrication of graphene-based electrode in less than a minute through hybrid microwave annealing. Sci Rep. 2015;4(1):5492.
- Li F, Ye J, Zhou M, Gan S, Zhang Q, Han D, et al. All-solid-state potassium-selective electrode using graphene as the solid contact. Analyst. 2012;137(3):618–23.
- Fouskaki M, Chaniotakis N. Fullerene-based electrochemical buffer layer for ion-selective electrodes. Analyst. 2008;133(8):1072–5.
- Bono MJ, Reygaert WC. Urinary tract infection. [Internet]. StatPearls. StatPearls Publishing; 2021 [Cited 2021 Apr 16].
- Laboratory assessment of kidney disease. In: Pocket companion to Brenner and Rector's The kidney. Elsevier; 2011. p. 21–41.
- Wan Salim WWA, Hermann AC, Zietchek MA, Pfluger JE, Park JH, ul Haque A, et al. Ion-selective electrode biochip for applications in a liquid environment. In: International Conference for Innovation in Biomedical Engineering and Life. Sciences. 2016: 86–93.
- Han W-S, Chung K-C, Kim M-H, Ko H-B, Lee Y-H, Hong T-K. A hydrogen ion-selective poly(aniline) solid contact electrode based on dibenzylpyrenemethylamine Ionophore for highly acidic solutions. Anal Sci. 2004;20(10):1419–22.
- Piao M-H, Yoon J-H, Jeon G, Shim Y-B. Characterization of all solid state hydrogen ion selective electrode based on PVC-SR hybrid membranes. Sensors. 2003;3(6):192–201.
- Lewenstam A. Routines and challenges in clinical application of electrochemical ion-sensors. Electroanalysis. 2014;26(6):1171–81.
- Simonian AL, Good TA, Wang SS, Wild JR. Nanoparticle-based optical biosensors for the direct detection of organophosphate chemical warfare agents and pesticides. Anal Chim Acta. 2005;534(1):69–77.
- Haandel MJH. van. Structure, function and operational stability of peroxidases. PhD Thesis, Wageningen University, 2000. ISBN 9789058082855.
- Carnauba R, Baptistella A, Paschoal V, Hübscher G. Diet-induced low-grade metabolic acidosis and clinical outcomes: a review. Nutrients. 2017;9(6):538.
- Leonberg-Yoo AK, Tighiouart H, Levey AS, Beck GJ, Sarnak MJ. Urine potassium excretion, kidney failure, and mortality in CKD. Am J Kidney Dis. 2017;69(3):341–9.
- Udensi U, Tchounwou P. Potassium homeostasis, oxidative stress, and human disease. Int J Clin Exp Physiol. 2017;4(3):111.
- Aoi W, Marunaka Y. Importance of pH homeostasis in metabolic health and diseases: crucial role of membrane proton transport. Biomed Res Int. 2014;2014:1–8.

**Publisher's note** Springer Nature remains neutral with regard to jurisdictional claims in published maps and institutional affiliations.





Ivan Kucherenko was a joint PhD from Claude Bernard Lyon 1 University and Taras Shevchenko National University of Kyiv, and performed research at Iowa State University in the frame of a Fulbright scholarship. His research focused on the application of graphene-based electrodes and developing electrochemical biosensors for medical diagnostics, quality control of pharmaceuticals, and the monitoring of toxic compounds.



Alexander Wilkins is currently an undergraduate student in mechanical engineering at the University of Buffalo, and performed research funded by the National Science Foundation's Research Experiences for Undergraduates program at Iowa State University. His research focused on the development of lowcost, water splitting electrodes based upon graphene materials.



Bolin Chen is currently a postdoctoral scholar in the Pritzker School of Molecular Engineering at the University of Chicago. His research interests focus on the science, processing, and application of advanced manufacturing for energy and sensing applications.



Delaney Sanborn is a doctoral student in mechanical engineering at the University of Minnesota and worked as an undergraduate researcher on this project while studying at Iowa State University. Her research areas include the fabrication of devices and sensors with nanomaterials for biomedical and environmental applications.



Zachary Johnson is currently a graduate researcher in mechanical engineering at Iowa State University. His work consists of micro- and nanoscale fabrication of graphene-based materials through various printing and laser techniques while additionally working with bioderived substrates and inks that can be used for environmental sensing.



Natalie Figueroa-Felix is an undergraduate student at Iowa State University majoring in mechanical engineering. Her research interests focus on the application of sensors and how they can be applied to the pharmaceutical sciences industry.





Deyny Mendivelso-Perez received her PhD in analytical chemistry from Iowa State University and specializes in chromatography and mass spectrographic methods as well as ionic liquids. She focused on understanding separation systems that utilize ionic liquids by varying and tuning the physical properties of those liquids.



Carmen L. Gomes is Associate Professor in the Mechanical Engineering Department at Iowa State University where she is leading her research program on the design of novel nanoscale materials using biopolymers and 2D materials for the development of functional delivery systems and biosensors for food and agricultural applications.



Emily Smith is Professor of Chemistry at Iowa State University and the Division Director for Chemical and Biological Sciences at Ames Lab, a US Department of Energy National Laboratory. Her research interests are optical spectroscopy instrument development for the analysis of nanoscale phenomena and materials.



Jonathan C. Claussen is Associate Professor in the Mechanical Engineering Department at Iowa State University. His research interests are in the fabrication of nanomaterials and nanostructured devices for a wide variety of applications including biosensors, energy harvesters, and cellular interface materials. His laboratory specializes in developing flexible graphene-based biosensors developed from inkjet and aerosol printing as well as through laser writing.

